Energy parasites trigger oncogene mutation

Supplement to the manuscript

Cancer is a problem including defects of biological, biochemical, and biophysical processes (Pokorný et al. 2013, 2015). Cancer initiation described in the presented paper corresponds to this interdisciplinary concept. To facilitate understanding of particular steps of cancer initial development along the cancer transformation pathway, an overview of important processes published in different papers was prepared and included in this supplement. The biological experimental part is based on measurement of the cell-mediated immunity, the biophysical part includes effect of parasitic virus energy consumption and the biochemical part describes Stark effect in chemical reactions.

Measurement of the cell-mediated immunity

Introduction

Overview of the cell-mediated immunity (CMI) of healthy humans, precancerous and cancer patients is based mainly on papers (Jandová et al. 2001, 2009a, 2009b). CMI is understood to correlate with adherence properties of leukocytes (from peripheral blood) to solid state surfaces. LAI (leukocyte adherence inhibition) assay is a quantitative technique that was widely used to study and monitor the CMI (Halliday et al. 1972, Holáň et al. 1974, Koppi et al. 1974, Grinnell 1978, Witkowski et al. 1972). The LAI assay is based on observation of *in vitro* adherence of leukocytes to surfaces of glass or some plastic materials in the presence and in the absence of antigens. CMI response to antigens is related to specific processes in cells which are under immune surveillance and, therefore, displays transferred information about their state and evolution. But the LAI assay method is complex and tedious, and unequivocal results are conditioned by high purity of antigens used, i.e. the most immunoactive components have to be separated, and by experienced visual microscopic evaluation. Antigen alters adherence after it binds to corresponding receptor in the cellular membrane. Not only chemical but also physical agents can affect CMI and change adherence of T lymphocytes. Numerous experimental LAI assays were made for a quantitative examination of adherence of T lymphocytes to assess tumor-specific CMI (Bugger et al. 2008, Gipson et al. 1978, Grosser et al. 1975, Hellstroem et al. 1976, Marti et al. 1976, Noonan et al. 1977, Shani et al. 1978, Tataryn et al. 1978, Thomson et al. 1979). We studied CMI in healthy humans and cancer (Ca) patients with gynaecological and otorhinolaryngological (ORL) tumors using specific antigens prepared from corresponding cancer tissues and non-specific antigen prepared from plasma of mice infected with lactate dehydrogenase-elevating virus (LDH) by high-pressure gel chromatography.

As the purified antigens and other measures have made possible high reliability and reproducibility of the LAI assay results in our laboratory, we performed investigations for

more than three decades and accumulated considerable amount of data on CMI in healthy humans and cancer patients (Jandová et al. 1979, 1996, 1999, 2001, 2004, 2005, 2009a, 2009b). Association of the CMI response to the non-specific antigen with pathology of the cellular energy production was an original contribution published in the article Disease of the Cellular Energy System (Jandová et al. 1979). Therefore, our experimental investigations were underlain by a hypothesis that CMI response to the non-specific antigen discloses defects of oxidative mitochondrial function which is a common *denominator* of a group of diseases of the cellular energy production system. CMI response to non-specific antigen was examined in acute myocardial infarction (AMI) and schizophrenia (Sch) patients too. The CMI data are presented in this paper with discussion of processes which are assumed to be monitored by the response to the non-specific antigen.

Materials and methods

T cells were separated from venous blood of healthy humans and cancer patients. Histopathological verification of the cancer diagnosis was made.

Cervical precancerous lesions were diagnosed by cytological (PAP) smears, from examination by colposcopy, and from colposcopically directed *punch* biopsy material by histology. Cytology and colposcopy revealed suspect cervical lesions which were exactly classified by biopsy. The grades of development of precancerous lesions LSIL and HSIL (low and high-grade squamous intraepithelial lesions, respectively) were determined by cytology, and CIN1, CIN2, and CIN3 (cervical intraepithelial neoplasia) grades by histology. Cytology and colposcopy diagnostic results in HSIL grade correspond to CIN2 and CIN3 grades. Persisting LSIL with HPV infection indicates increased probability for development of CIN2 or CIN3 lesions (Solomon et al. 2001).

Preparation of T cells

Eight millilitres of venous blood was taken from the patient and transferred to a test tube with 500 U of heparin and incubated in a water bath for 30 min at 37ºC. A Pasteur pipette was used to transfer the plasma rich in white blood cells into a new test tube. The contents were diluted with saline solution or phosphate buffered saline (PBS), minimum essential medium (MEM), medium to its original volume and centrifuged at 1800 rpm. The supernatant was poured off and the sediment was layered with 1 ml of distilled water, bubbled through a Pasteur pipette, and lysis of erythrocyte was achieved. Thereafter, dilution to volume with some of the above-mentioned solutions according to an option was done. Thus, the lysis of erythrocyte was stopped. The contents were centrifuged once again for 10 min at 1800 rpm. The rinsing solution was poured off, the sediment of white blood cells was diluted with a selected medium, filtered through nylon absorbent wool (resulting in enrichment of the T cells), and

diluted again so as to make available 4×10^6 cells per ml for the test, as counted in a Bürker chamber.

For purification of T cells, we used a 5-cm^3 syringe filled with nylon absorbent wool as a filtration column. The pool passing through the column contained about 92% of T cells and 8% of other cells (Tlaskalová–Hogenová et al. 1980).

Preparation of the immunoactive fraction from malignant tumor (specific antigen)

The biological material was taken during surgery, in cooperation with a histopathologist, and placed into a sterile vessel in dry ice. After the material was defrosted, fat and/or necrotic parts were removed. Homogenization was then carried out, and the homogenate was cryolyzed three times at –60 and +40ºC. Thereafter, it was centrifuged 3.5×10^3 ×g at +4ºC for 40 min. The supernatant was subjected to centrifugation again at 10^5 ×g at +40ºC for 60 min. The supernatant, which contains proteins, nucleoproteins, nucleic acids, and low molecular weight components was extracted with phenol for 15 min at ambient temperature at a volume ratio of 1:1 in the presence of 1% sodium dodecylsulfate and 0.01% of 8-hydroxyquinoline, and pH was adjusted to 7–7.5.

By means of centrifuge at 3×10^3 ×g the aqueous phase was separated and shaken again with phenol. The aqueous phase, containing a mixture of cytoplasmic ribonucleic acids, was further separated on a column filled with oligo-dT-cellulose (cellulose with bound deoxythimidine oligonucleotides) having affinity for polyadenylated remnants characteristic of information ribonucleic acids. The polyadenylated ribonucleic acids captured on the column were rinsed with water, and the aqueous eluate was purified with high-pressure gel chromatography. The column was filled with Separon-Hema-300 glc® gel, which is a suspension copolymer of 2-hydroxyethyl-methacrylate with ethylenedimethacrylate with an exclusion limit of 3×10^5 kDa.

Detection was carried out by means of an R 043 differential refractometer and a UV flow-through spectrophotometer with variable wavelength. Saline solution was used as a mobile phase. Immunologically active and organ specific antigens were obtained in a 25–50 cm^3 fraction of the eluate evaluated at the wavelength of 340 nm.

Preparation of the immunologically functional fraction from the inbred strain mice serum (non-specific antigen – LDH antigen)

The immunologically functional fraction was obtained from the serum of inbred laboratory mouse strain, e.g., C3H infected with the virus (LDH) enhancing the lactate dehydrogenase isoenzyme. Plasma obtained from blood treated with heparin was subjected to at least doubled centrifugation for 20–30 min at $3–3.5 \times 10^3$ ×g, and the supernatant taken was then clarified

for 1–2 min at 9–11 × 10^3 ×g. The supernatant was subjected to further centrifugation for 50–100 × 10^3 ×g, and the sediment was suspended in buffer with pH of 7–7.4 consisting of tris-(hydroxymethyl)-aminomethane-NaCl [tris-NaCl] and the disodium salt of ethylenediaminetetraacetic acid (EDTA) in a minimum volume of at most 1 ml. Equilibrium centrifugation in a saccharose density gradient separated the constituents, and the area corresponding to 32–38% saccharose with the maximum at 35% saccharose. This fraction was taken off and, after dilution with the above-mentioned buffer at a volume ratio of 1:0.5 to 1.5, was subjected to centrifugation at 50–100 × 10^3 ×g, for 50–70 min. Manipulation of blood plasma until obtaining the last sediment was carried out at 2–6ºC. The sediment obtained was dissolved in 1.5–3.0 ml of saline solution and used for high pressure gel chromatography. The fractions corresponding to molecular masses of 3×10^5 to 1.5×10^4 kDa were immunologically active. The equilibrium centrifugation was carried out for a period of 180–210 min at 150–180×10^3 ×g. Separon Hema-300 glc®, which is a suspension copolymer of 2-hydroxyethyl-methacrylate with ethylenedimethacrylate with an exclusion limit of the column of 3×10^5 kDa, was used as the stationary phase for the high-pressure gel chromatography. Gel particle size was 32–40 μm. A differential refractometer and a UV spectrophotometer with variable wavelength were used for detection. Saline solution was used as a mobile phase, and the active fraction was found using a wavelength of 340 nm.

Experimental results

To elicit the immune reaction, the T cells prepared according to the method described above were mixed with antigen (specific or non-specific) at a ratio of 1 part of antigen to 4 parts of T cell float. Antigen was mixed with the suspension just before starting the experiment.

Concentration of antigens was determined as milligrams per millilitre. The same exposure conditions were used for T cells from healthy humans and from cancer patients. Leukocyte-mediated immunity was assessed by the LAI assay. The number of non-adherent T cells in suspension was counted after 1 hour of sedimentation.

The relative frequency p/N of occurrence of the LAI assays whose number of non-adherent lymphocytes is in the region from M to $M + \Delta M$, where $\Delta M = 2\%$ and p is the frequency of occurrence and N is the total number of experiments. Significant differences exist between LAI assay results measured on lymphocytes taken from healthy humans versus those from cancer patients illustrated in Fig. 1. The data plotted in Fig. 1 represent LAI experimental results measured and evaluated from 1976 till the end of 2000 published in (Jandová et al. 2009b). Data measured in the period 1976–1992 were included in (Jandová et al. 2001). There are only small differences in the plotted curves.

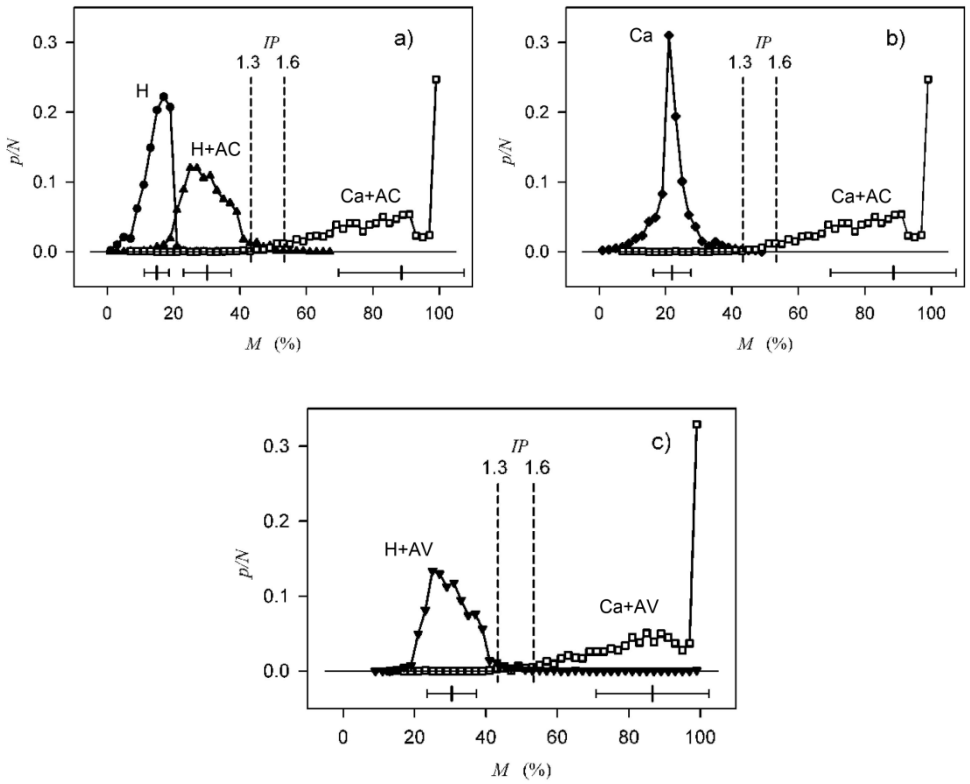


Fig. 1 The relative frequency p/N of cases as a function of the number M of non-adherent T lymphocytes (the experimental values connected with lines). T lymphocytes were taken from 1) healthy humans and examined without antigen – H, $N_H = 1721$ (a), with specific antigen – H+AC, $N_H(+AC) = 3071$ (a), and with non-specific (LDH virus) antigen – H+AV, $N_H(+AV) = 1960$ (c); 2) cancer patients and examined without antigen – Ca, $N_{Ca} = 1100$ (b), with specific antigen – Ca+AC, $N_{Ca}(+AC) = 1949$ (a, b), and with non-specific antigen – Ca+AV, $N_{Ca}(+AV) = 2298$ (c). The dashed vertical lines denote the principle normalized values of M (i.e. $IP = 1.3$, and $IP = 1.6$) which determine the assumed noise region. Circles, triangles up, triangles down, diamonds, and squares denote the evaluated values of H, H+AC, H+AV, Ca, and Ca(+AC) or Ca(+AV), repectively. The short vertical lines connected with horizontal lines under the p/N curves denote their mean values and standard deviations. (Courtesy of the journal Neural Network World.)

The p/N values of the cervical precancerous lesions are distributed in the whole spectrum of M. Precancerous lesions enable us to follow and analyze a certain period of cancer transformation before the final pathological product is formed—a malignant cell. In the cervical precancerous evolution period the immune system is able to suppress the cancer development and the probability of successful cancer eradication is not negligible. Nevertheless, behavior of precancerous events is unpredictable and invasive carcinoma may develop from any level of abnormalities (Koss 1997). Cervical carcinoma cells fail to induce an effective specific cytotoxic T lymphocyte response and tumor cells escape host immune

surveillance (Kaufmann et al. 1996). Cell-mediated immunity response of the healthy humans and of cancer patients examined by LAI assay displays large statistically significant differences for both antigens. CMI response to the specific and non-specific antigen seems to be similar for healthy humans as well as for cervical carcinoma patients but the differences are statistically significant. Therefore, the specific and the non-specific antigen may monitor the same pathological process but elicit responses of different magnitude, but we also have to admit that the antigens monitor different processes and trace different parts or branches of the carcinogenesis pathway. However, both antigens represent the active fraction of the eluate evaluated at the same wavelength 340 nm. This coincidence suggests that their difference is not principal. The specific antigen may contain a specific cancer code. As LDH virus is a parasite on the energy system of infected cells, the process monitored by the non-specific antigen might be of the same nature—might detect oxidative energy production, i.e. mitochondrial activity.

The Stark effect

Effect of static electric field

A short basic overview of the Stark effect is included. Effect of external electric field on energy levels of microsystems was observed and described by J. Stark (1914). Spectral lines of atoms and molecules are shifted and split by external electric field. The formerly degenerated energy levels are split into lower and higher energy levels. Splitting of output spectra is caused by changes of energy levels. Energy of electrons at atomic and molecular orbitals is affected by the electric field. The higher the energy of electrons, the smaller the Stark effect. Therefore, electrons on outer orbitals are more susceptible to the effect of electric fields. A large effect of the electric field may be exerted on weakly bound electrons on outer molecular orbitals. A strong oscillating electric field can also supply energy and overlay oscillations on electrons at low energy levels.

The vibrational Stark effect consists of a shift of certain vibration modes due to exposure to local electric field. The Stark effect for a vibrational transition in a protein was described by Park et al. (1999). The field is collectively called the matrix electric field E_{m} and the observed electrochromic band shift (corresponding to a frequency shift) $\Delta W = -\Delta\zeta E_{\mathrm{m}}$ where $\Delta\zeta$ is a change in dipole moment associated with a spectroscopic transition. The Stark spectroscopy of electronic transitions in proteins is now a standard method. The vibrational Stark Effect is exploited for measurement of the local electric field in chemical structures (Schkolnik et al. 2012). The Stark probes have been recently employed to investigate electric fields in the active sites of proteins and enzymes as well as conformational changes in proteins. Vibrational Stark effect spectroscopy reveals electrostatic mechanism for protein-protein interaction (Stafford et al. 2010).

Effect of oscillating electric field

Shift and splitting of spectral lines and shift of frequencies of vibrations are typical examples of physical changes of microscopic energy levels caused by the electric fields. Energy changes of the bonding electrons resulting in increased or decreased probability of bonding seems to be another consequence of the electric field activity. Effect of local electric field on enzymatic reaction described by Fried et al. (2014) is a special case of the Stark effect resulting in acceleration of reactions (Hildebrandt 2014). Oscillating electric field generated by electric polar vibrations in living cells may also affect probability of bonding. The final effect may depend on energy and frequency of oscillations.

A useful concept of bonding may be derived from electron orbitals of interacting molecules. A quantitative assessment may be yielded by the overlap integral. Increase of electron energy and oscillatory features of behavior can be inscribed into wave functions of electrons. The overlap integral is given by (Streitwieser 1962)

$$S = \int \Psi_a \Psi_b d\tau$$

where indicess *a* and *b* denote different electrons (the complex conjugate is not denoted). The integral is a function of space distribution of the normalized wave function Ψ_a and Ψ_b, i.e. of the distance between the electrons. For $a = b$ the normalization condition $S = 1$ is valid. The relation between overlapping and the bond energy is based on the principle of maximum overlapping. This principle states that the bond strength increases with decreasing distance between bonding electrons.

Effect of oscillating electric field on bonding strength is a special case of the overlapping process. The bonding electrons may exhibit correlated motion and the probability of bonding may be high. For assessment of this case a four-dimensional space model is suggested with time as the fourth dimension. The wave functions Ψ_a and Ψ_b can be replaced by normalized superposition of two wave functions in the form ${}^{\alpha}\Psi_a(\tau) + {}^{\beta}\Psi_a(t, \tau)$ and ${}^{\alpha}\Psi_b(\tau) + {}^{\beta}\Psi_b(t, \tau)$ where α and β indices denote terms related to Ψ_a, Ψ_b and terms produced by the oscillating dipole, respectively. After substitution into the overlap integral the results are

$$S_{\alpha} = \int {}^{\alpha}\Psi_a(\tau)\, {}^{\alpha}\Psi_b(\tau)\, dt\, d\tau ,$$
$$S_{\alpha\beta} = \int [{}^{\alpha}\Psi_a(\tau)\, {}^{\beta}\Psi_b(t, \tau) + {}^{\beta}\Psi_a(t, \tau)\, {}^{\alpha}\Psi_b(\tau)]\, dt\, d\tau ,$$
$$S_{\beta} = \int {}^{\beta}\Psi_a(t, \tau)\, {}^{\beta}\Psi_b(t, \tau)\, dt\, d\tau.$$

For ${}^{\beta}\Psi_a(t, \tau) = 0$ and ${}^{\beta}\Psi_b(t, \tau) = 0$ the terms $S_{\alpha\beta} = S_{\beta} = 0$, ${}^{\alpha}\Psi_a(\tau) = \Psi_a / k$, ${}^{\alpha}\Psi_b(\tau) = \Psi_b / k$ and $S_{\alpha} = S$ where *k* is the integration constant. If the terms $S_{\alpha\beta} + S_{\beta}$ are larger than the term S_{α} the role of the oscillation field is dominant and a probability of bonding is high. In the opposite

case the probability of bonding is low. This type of the Stark effect depends on oscillations of the electric field generated by polar vibrations and might be termed as a *reverse vibrational Stark effect*.

Field generation in a cell

Oscillating electric fields in eukaryotic cells is generated by microtubules. Vibrations and excitation of oscillating electric fields are spread in the cell and in the biological system and the vibrating dipoles and multipoles generate in-phase oscillating electric field. The near electric field of microtubules may be assessed from the electric field generated by a model structure of nine oscillating dipoles located in positions corresponding to the centers of the neighboring heterodimers in a microtubule. The generated field is evaluated up to a distance of 30 nm and plotted in Fig. 2. The dipole moment is given by *Qd*, where *Q* is formed by elementary charges (18 calcium ions and corresponding number of electrons) and *d* is the amplitude of vibrations. All interacting macromolecules are in the oscillating field of the whole cell and chemical bonding is affected if the intensity of the field is sufficiently high.

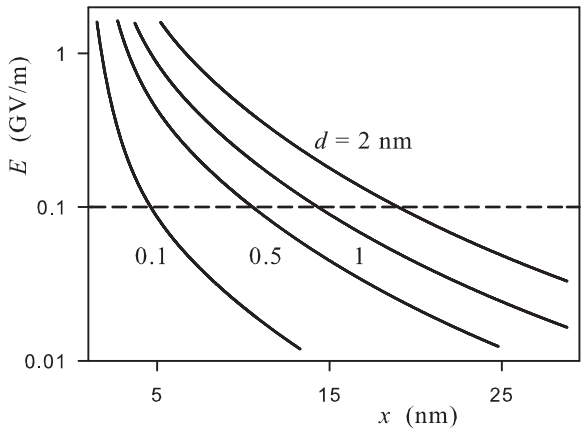


Fig. 2: Intensity of the near electric field around a dipole model of a part of microtubule surface as a function of the distance. The dipole is formed in each heterodimer by the charges of Ca ions and equivalent charge of electrons; *d* is the amplitude of the charge oscillation.

Experimental investigation of the microtubule electromagnetic activity is at the initial phase. Sahu *et al.* (2013, 2014) measured resonant frequencies of isolated microtubules in the frequency range of about 0.1–0.4 MHz, 10–30 MHz, 100–200 MHz, 1–20 GHz, at approximately 20 THz (wavenumber about 700 cm^{-1}), and the UV absorption-emission spectrum around 300 nm. Electromagnetic field (oscillating electric field) at the cellular membrane was measured and described in (Pokorný et al. 2001, Hölzel 2001). Electromagnetic signal at the cell surface in the frequency range 8–9 MHz was embedded in noise and thus assessment of power was imposible. Hölzel (2001) disclosed electric

oscillations in the frequency range 1.5–52 MHz using a special detection and amplification system. However, the measurement was also targeted to prove the existence of the cellular vibrations. The amplitude of cellular membrane vibrations (i.e. microtubule vibrations) was measured. Their highest amplitude at the membrane of a human cell (cantilever deflections) is about 5 nm (Kasas et al. 2015). A microtubule 8 μm long contains 10^3 spiral heterodimer levels. If all heterodimers oscillate in phase then their amplitudes of vibrations $A = 0.005$ nm. Interaction between vibrating Ca ions and electrons in heterodimers may be described by a momentum relation

$$m_e \int \mu_e E(t)dt = m_n \int \mu_n E(t)dt = m_n A$$

where m_e, m_n, and μ_e, μ_n are the effective masses and the mobilities of electrons and Ca ions in heterodimers, respectively (the term mobility of Ca ions is introduced by analogy with that of electrons). The integral is assumed to be evaluated in a quarter of a period of harmonic oscillations. The effective mass of Ca ions is much higher than that of electrons. Therefore, their amplitude of oscillations might be at least 100 times higher than the amplitude of vibration A and thus $d \sim 0.5$ nm. However, if the electrons are weakly bonded then the amplitude d may be higher.

References

Bugger H, Abel ED. 2008. Molecular mechanisms for myocardial mitochondrial dysfunction in the metabolic syndrome. Clin Sci 114:195–210.

Fried SD, Bagchi S, Boxer SG. 2014. Extreme electric fields power catalysis in the active site of ketosteroid isomerase. Science 346:1510–1514.

Gipson TG, Martin WJ. 1978. In vivo Anti-Tumor Immunity Detected by Leukocyte Adherence Inhibition. Cancer Immunol Immunother 3:201–205.

Grinnell F. 1978. Cellular Adhesiveness and Extracellular Substrata. In: Int. Rev. Cytol., Bourne GH, Danielli JF, editors. New York: Academic Press 53. p.65-144.

Grosser N, Thomson DMP. 1975. Cell-mediated Antitumor Immunity in Breast Cancer Patients Evaluated by Antigen-induced Leukocyte Adherence Inhibition in Test Tubes. Cancer Res 35:2571–2579.

Halliday WJ, Miller S. 1972. Leukocyte adherence inhibition: a simple test for cell-mediated immunity and serum block factors. Int J Cancer 9:477–483.

Hellstroem I, Hellstroem KE, Shantz G. 1976. Demonstration of Tumor-Associated Immunity with a Leukocyte Adherence Inhibition (LAI) Assay. Int J Cancer 18:354–361.

Hildebrandt P. 2014. More than fine tuning. Science 346:1456–1457.

Holáň V, Hašek M, Bubeník J, Chutná J. 1974. Antigen mediated macrophage adherence inhibition. Cell Immunol 13:107–116.

Hölzel R. 2001. Electric Activity of Non-Excitable Biological Cells at Radio Frequencies. Electro- Magnetobiol 20:1–13.

Jandová A, Motyčka K, Čoupek J, Sanitrák J, Heyberger K, Laurová, et al. 1979. "Disease" of the Cellular Energy System. Sborník lékařský 81:321–327 (in Czech).

Jandová A, Kobilková J, Nedbalová M, Šorfová J, Dohnalová A, Trojan S., Pokorný J. 1996. Study of interaction forces in human CD4Ly. Bioelectrochem Bioenerg 41:181–185.

Jandová A, Hurych J, Nedbalová M, Trojan S, Dohnalová A, Čoćek A, et al. 1999. Effects of sinusoidal magnetic field on adherence inhibition of leukocytes: preliminary results. Bioelectrochem Bioenerg 48:317–319.

Jandová A, Hurych J, Pokorný J, Čoček A, Trojan S, Nedbalová M, Dohnalová A. 2001. Effects of Sinusoidal Magnetic Field on Adherence Inhibition of Leukocytes. Electro-Magnetobiol 20:397–413.

Jandová A, Pokorný J, Čoček A, Trojan S, Nedbalová M, Dohnalová A. 2004. Effects of Sinusoidal Magnetic Field 0.5 mT on Leukocyte Adherence Inhibition. Electromagn Biol Med 23:81–96.

Jandová A, Mhamdi L, Nedbalová M, Čoček A, Trojan S, Dohnalová A, Pokorný J. 2005. Effects of Magnetic Field 0.1 and 0.05 mT on Leukocyte Adherence Inhibition. Electromagn Biol Med 24:283–292.

Jandová A, Pokorný J, Kobilková J, Janoušek M, Mašata J. Trojan S et al. 2009a. Cell-Mediated Immunity in Cervical Cancer Evolution. Electromagn Biol Med 28:1–14.

Jandová A, Pokorný J, Kobilková J, Trojan S, Nedbalová M, Dohnalová A, et al. 2009b. Mitochondrial dysfunction. Neural Netw World 19:379–391.

Kasas, S, Ruggeri FS, Benadiba C, Maillard C, Stupar P, Tournu H, et al. 2014. Detecting nanoscale vibrations as signature of life. Proc Natl Acad Sci USA 2015;112:378–381.

Kaufmann AM, Gissmann L, Street D, Schreckenberger C, Hunter M, Qiao L. 1996.

Expression of CD80 Enhances Immunogenicity of Cervical Carcinoma Cells in Vitro. Cell Immun 169:246–251.

Koppi TA, Maluish AE, Halliday WJ. 1979. The cellular mechanism of leukocyte adherence inhibition. J Immunol 123:2255–2260.

Koss LG. 1997. Precancerous Lesions of the Epithelia of the Uterine Cervix. Compendium on Diagnostic Cytology. The Tutorials of Cytology, Inter Acad Cytology 86–94.

Marti JH, Thomson DMP. 1976. Anti-Tumour Immunity in Malignant Melanoma Assay by Tube Leucocyte Adherence Inhibition. Brit J Cancer 34:116–133.

Noonan FP, Halliday WJ, Wall DR, Clunie GJA. 1977. Cell-mediated Immunity and Serum Blocking Factors in Cancer Patients during Chemotherapy and Immunotherapy. Cancer Res. 37:2473–2480.

Park ES, Andrews SS, Hu RB, Boxer SG. 1999. Vibrational Stark Spectroscopy in Proteins: A Probe and Calibration for Electrostatic Fields. J Phys Chem B 103:9813–9817.

Pokorný J, Hašek J, Jelínek F, Šaroch J, Palán B. 2001. Electromagnetic Activity of Yeast Cells in the M Phase. Electro- Magnetobiol 20:371–396.

Pokorný J, Pokorný J, Kobilková J. 2013. Postulates on electromagnetic activity in biological systems and cancer. Integrat Biol. 5:1439–1446.

Pokorný J, Pokorný J, Foletti A, Kobilková J, Vrba J, Vrba Jr. J. 2015. Mitochondrial dysfunction and disturbed coherence: Gate to cancer. Pharmaceuticals 8:675–695.

Sahu S, Ghosh S, Ghosh B, Aswani K, Hirata K, Fujita D, Bandyopadhyay A. 2013. Atomic water channel controlling remarkable properties of a single brain microtubule: Correlating single protein to its supramolecular assembly. Biosens Bioelectron 47: 141–148.

Sahu S, Ghosh S, Fujita D, Bandyopadhyay A. 2014. Live visualizations of single isolated tubulin protein self-assembly via tunneling current: Effect of electromagnetic pumping during spontaneous growth of microtubule. Sci Rep 4:7303.

Schkolnik G, Salewski J, Millo D, Zebger I, Franzen S, Hildebrandt P. 2012. Vibrational Stark Effect of the Electric-Field Reporter 4-Mercaptobenzonitrile as a Tool for Investigating Electrostatics at Electrode/SAM/Solution Interfaces. Int J Mol Sci 13(6):7466–7482.

Shani A, Ritts RE, Thynne GS, Weiland LH, Silvers A, Moertel ChG, Go VLW. 1978. A Prospective Evaluation of the Leukocyte Adherence Inhibition Test in Colorectal Cancer and Its Correlation with Carcinoembryonic Antigen Levels. Int J Cancer 22:113–119.

Solomon D, Schiffman M, Tarone R. 2001. Comparison of three management strategies for patients with atypical squamous cells of undetermined significance: Baseline results from a randomized trial. J Natl Cancer Inst 93:293–299.

Stafford AJ, Ensign DL, Webb LJ. 2010. Vibrational Stark Effect Spectroscopy at the Interface of Ras and Rap1A Bound to the Ras Binding Domain of RalGDS Reveals an Electrostatic Mechanism for Protein-Protein Interaction. J Phys Chem B 114: 15331–15344.

Stark J. 1914. Observations of the effect of the electric field on spectral lines I. Transverse effect. Ann. Phys. 43:965–983 (in German).

Streitwieser A. 1962. Molecular Orbital Theory. New York – London (GB): Wiley.

Tataryn DN, Macfarlane JK, Thomson DMP. 1978. Leukocyte Adherence Inhibition for Detecting Specific Tumour Immunity in Early Pancreatic Cancer. Lancet 311 (8072):1020–1022.

Thomson DMP, Tataryn DA, Schwartz R, MacFarlane JK. 1979. Abrogation of the Phenomenon of Leukocyte Adherence Inhibition by Excess Circulating Tumour Antigen. Europ J Cancer 15:1095–1106.

Tlaskalová–Hogenová H, Čoupek J, Pospíšil M, Tučková I, Kamínková J, Mančal T. 1980. Affinity Chromatography of Human Lymphocytes on Spheron Immunoadsorbent Column. J Polym Sci 68:89–95.

Witkowski JA, Brighton WD. 1972. Influence of serum on attachment of tissue cells to glasssurfaces. Exp Cell Res 70:41–48.